Nanofabricated Low-Voltage Gated Si Field-Ionization Arrays

Nanofabricated Low-Voltage Gated Si Field Ionization Arrays

Girish Rughoobur, Álvaro Sahagún, Olusoji O. Ilori, and Akintunde I. Akinwande

***Abstract*—We demonstrate high density (1 µm pitch) silicon field ionization arrays (FIAs) with self-aligned gate apertures (350 nm in diameter) and integrated nanowire current regulators. Our FIAs achieved high field factors (>0.1 nm^{-1} and significantly lower ionization voltages (<100 V) than devices with lower tip densities previously reported. Ion currents were measured in argon, deuterium and helium at pressures from 1 mTorr to 16 mTorr. The FIAs turned on between 70-85 V and, ion currents of around 0.4 nA were measured at 100 V. Higher currents of 7 nA were obtained at 147 V and 16 mTorr, but with the risk of gate damage by ions energized in the intense gate-ionizer field. Si FIAs coated with Pt resulted in higher field factors due to sharper tips, but lower ion currents. Surface states, coupled with molecular adsorption and transport to the ionizer are the possible mechanisms for lower voltage ionization in uncoated Si FIAs.**

***Index Terms*—Ionization, ion sources, vacuum microelectronics, nanotechnology**

I. Introduction

SINCE the first observation of field ionization by Müller [1] in 1957, devices that can field-ionize gas molecules have found applications in mass spectrometry [2], neutron sources [3], gas sensors [4], field ion microscopy [5] and scanning helium ion microscope [6]. The field ionization (FI) mechanism consists of a valence electron from a gas atom or molecule tunneling across a potential barrier, into a vacant electron state in a pointed electrode called here an "ionizer" [7]. Compared to electron impact ionization [8] and chemical ionization [9] methods, FI results in the controlled formation of ion species without the possibility of molecular fragmentation, even at higher pressures [2]. This is especially important for mass-spectrometry and sensing applications in order to analyze long-chain molecules without breaking up in smaller indistinguishable molecular fragments [10]. However, ion sources based on FI require extremely high positive electric fields, of the order of 10 V·nm^{-1} [11]. Such intense fields are only produced in the proximity of very sharp electrodes under extremely large voltage bias, which can be unsafe or can damage the electrodes due to the formation of energetic ions [12]. Ion sources based on microwave plasma generation with lower voltages have demonstrated high currents and high current densities; yet they are large and require strong magnetic fields [13].

G. Rughoobur, O. O. Ilori and A. I. Akinwande are with the Microsystems Technology Laboratories, Massachusetts Institute of Technology, 60 Vassar Street, Cambridge, MA 02139, USA. E-mail: grughoob@mit.edu

Á. Sahagún is with the Department of Electrical and Computer Engineering, University of Illinois at Chicago, 851 South Morgan Street, Chicago, IL 60607, USA.

Manuscript received Month Date, Year; revised Month Date, Year.

High-density sharp electrodes with a gated structure, pioneered by the Spindt-type Mo cathodes in 1968, have emerged as ideal candidates for field emission and field ionization as they are programmable and have instant response [14]. Compared to planar electrodes, the short distance between the gate and the nm-size tip allows Spindt-type devices to achieve the minimum ionization field, necessary to narrow the potential barrier, at lower voltages [15]. In particular, ionizers with self-aligned gates can generate this electric field at considerably lower bias as the separation between the gate and ionizer apex is uniform and shorter [16], [17]. Si field ionizers have further merits such as their compatibility with complementary metal-oxide semiconductor (CMOS) technology and the ability to form atomically sharp tips by oxidation [18]. Nonetheless, the two main limitations reported are the early tip burn-out due to the non-uniform tip distribution and premature breakdown voltages (∼75 V) in field emission [19]. A high aspect ratio nanowire (NW) current-limiter is integrated with the tip to regulate the current, hence compensating for the tip fabrication non-uniformity [20]. This NW can also increase the path length between the gate and the ionizer, which increases the breakdown voltage [3], [21]. Low voltage dielectric breakdown can also be circumvented by employing a mesa structure, which is formed by a highly anisotropic etch in conjunction with a thick oxide (>2 µm) holding the contact pads [21].

Such devices, as illustrated in Fig. 1, have already demonstrated high current densities, J, in field emission (FE) configuration, achieving $J > 100$ A·cm^{-2} and lifetime longer than 100 hours [22]. The NW current-limiters are approximately 8 µm in height, 1 µm apart (tip density of 10^8 cm^{-2}) and 100-200 nm in diameter, as shown by the scanning electron microscope (SEM) images in Fig. 1 (b) and Fig. 1 (c). A dielectric matrix of (SiN_x/SiO_2) supports the poly-Si gate while a 3 µm thick oxide holds the metal contacts. Previous works have reported that the tip radius has a log-normal distribution varying from 2 to 8 nm with a mean of 5 nm and a standard deviation of 1.5 nm, while the gate aperture is ∼350 nm in diameter and therefore, this structure results in field factors, β, exceeding 0.1 nm^{-1} [22], [23]. In this work, we use two key characteristics of this unique device architecture for field ionization arrays (FIAs): the densely-packed ionizers to increase the ion current, and the high field factors to reduce the minimum ionization voltage. We characterize the FI performance of the fabricated devices with gases that have a high first ionization energy —argon, deuterium and helium.

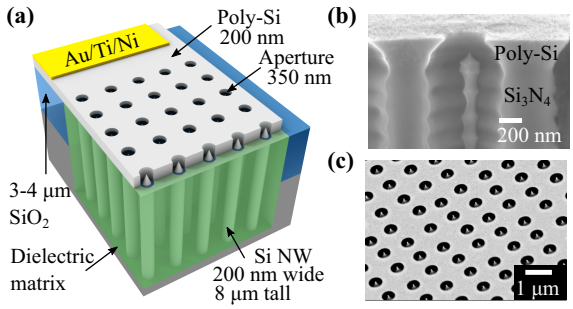

Fig. 1. (a) Schematic of the gated Si FIAs with a nanowire encapsulated in a dielectric matrix and a poly-Si gate for electron extraction. (b) Scanning electron microscope (SEM) cross-section of the tip and integrated nanowire with the oxide stripped for clarity. (c) SEM image of exposed Si FIAs with self-aligned apertures with 350 nm diameter.

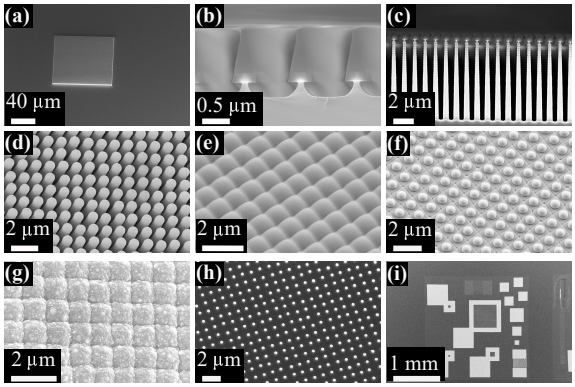

Fig. 2. Key fabrication steps: (a) formation of mesa, (b) tip definition, (c) nanowire etch, (d) oxidation sharpening, (e) low-stress nitride fill, (f) nitride planarization and etch-back, (g) poly-Si gate deposition, (h) aperture formation and, (i) metallization of gate for probe contact.

II. Experimental

A. Device Fabrication

The FIAs were fabricated on 150 mm diameter, 650 µm thick, ⟨100⟩ oriented *n*-type Si wafers and 1-4 Ω·cm resistivity. Key steps in the fabrication process are illustrated in Fig. 2. Mesas with depth of 3 µm were etched on the wafers and filled with 5 µm of SiO_2 by plasma enhanced chemical vapor deposition (PECVD). Chemical mechanical planarization (CMP) of SiO_2 was used to stop on the Si mesas. A hard mask of SiO_2 (150 nm thick) was then deposited by PECVD. The ionizer arrays (500 nm diameter discs and 1 µm pitch) were patterned by *i*-line UV photolithography using Microposit SPR700. The oxide caps were dry-etched before Si cones of ∼100 nm in diameter and 200 nm in height were fabricated by a semi-isotropic plasma etch based on SF_6/He. A highly anisotropic deep-reactive ion etch formed high aspect ratio (40:1) Si pillars of ∼8 µm in height. After removing the resist and oxide caps, the Si cones were sharpened to form tips by dry oxidation for 6.5 hours at 950 °C, which also narrowed the pillar (<200 nm). With low pressure chemical vapor deposition (LPCVD), the voids around the Si pillars were filled by a dielectric matrix of SiO_2 and low-stress SiN_x. CMP was used to planarize the SiN_x to within 200 nm of the tips and subsequently etched back using hot phosphoric acid at 165 °C to expose oxide domes of ∼250 nm in height. An 800 nm thick *n*-type doped poly-Si gate was deposited by LPCVD, and the gate apertures (∼350 nm in diameter) were carefully opened by CMP. Metal contacts were patterned using image reversal resist (AZ5214E), before depositing Ni/Ti/Au (10/20/200 nm) by electron beam evaporation. After lift-off, the backside of the wafer was etched to expose the Si. Ni/Al (50/100 nm) was deposited for the back contact and, the wafer was sintered at 400 °C in forming gas for 30 mins to reduce the contact resistance by forming nickel silicide. The process was completed by a 5 min dip in commercial pad etchant (Silox Vapox III) to expose the sharpened ionizers.

B. Electrical Characterization

Current-voltage (I-V) characteristics of fabricated FIAs were measured using three source-measurement units (SMUs) in an ultra-high vacuum (UHV) chamber, reaching a base pressure of 8×10^{-10} Torr. Vacuum was maintained by an ion pump and the pressure was recorded using a Bayard-Alpert ion gauge for FE measurements. Conversely for FI tests, vacuum was maintained using only a turbomolecular pump. The gas flow rate to reach the required pressure, p, was controlled by a precision needle valve from MDC Vacuum Products (Hayward, CA) and, p was measured using a convection Pirani gauge (Granville-Phillips® 275 Convectron®). Gases (Ar, D_2 and He) with 99.5% purity were purchased from Airgas (Radnor, PA, USA). D_2 is especially of interest as its ionization can produce neutrons for medical imaging and interrogation of radioactive materials [24]. Although the Pirani gauge was calibrated for N_2, the value of p for each gas was adjusted using the calibration plot (linear in the range of 0.1 mTorr to 0.1 Torr) from the manufacturer. The SMUs (Keithley Instruments, Model 237) were connected to the three-terminal device using miniature high voltage (MHV) feedthroughs and tungsten micro-manipulator probes. A stainless steel Faraday cup was used as the anode, positioned ∼3 mm from the FIAs and, biased at an anode voltage, V_A, of −200 V for FI. The Paschen curve for Ar has a minimum product of p and anode-gate distance, d, of 1 Torr·cm at a bias of 200 V [25]. In this work, the pd ranged from 10^{-4} to 10^{-3} Torr·cm based on values of d between 1 and 3 mm and, p in the range from 1 mTorr to 20 mTorr. Although V_A was kept at −200 V, this could be increased further without causing plasma discharge. For FI measurements, the extractor gate-emitter (V_{GE}) voltage was swept from 0 to −150 V, in 1 V steps, with the gate voltage, V_G, biased at 0 V; for FE, V_{GE} was swept from 0 to +60 V in 1 V steps, and V_A was +1100 V.

III. Results and Discussion

A. Field Factor

We modeled β using COMSOL Multiphysics® (v5.0) as shown in Fig. 3 to find the parameters, necessary to achieve the ionization field at low voltage. A 2D axis-symmetric geometry was implemented to reduce computation time. V_G and V_E were set to 0 V and +1 V, respectively to model the effects in FI mode. The apex of the tip was positioned at the same

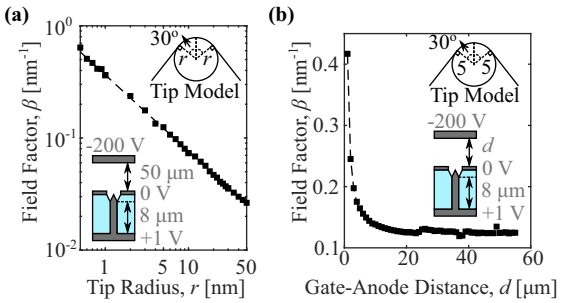

Fig. 3. Finite element modeling of field factor, β, using the Si FIAs. (a) Effect of tip radius, r, in nm on β with gate-anode separation, d of 50 μm and, (b) effect of d on β with $r = 5$ nm. Insets show simulation structure.

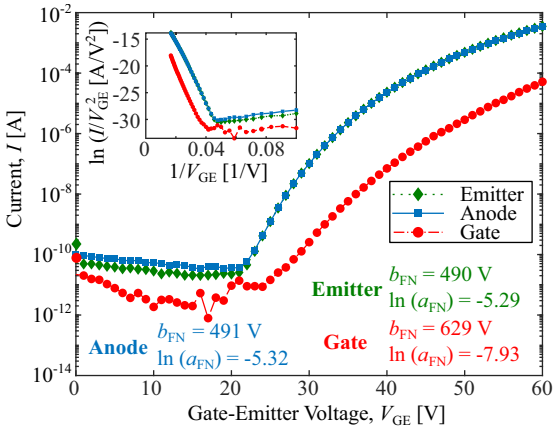

Fig. 4. (a) Field emission I-V transfer characteristics of a typical 1000×1000 array displaying the emitter, anode and, gate currents with anode voltage set to +1100 V. Inset shows corresponding Fowler-Nordheim (FN) plots with the extracted FN slope absolute values, $b_{\rm FN}$, and FN intercepts, $\ln(a_{\rm FN})$.

level as the base of the gate. A planar anode with $V_{\rm A}$ of -200 V, located at d of 50 μm away was added to evaluate the contribution of the anode to β. When the emitter-gate voltage, $V_{\rm EG}$, is 1 V, β is numerically equal to the electric field, F, at the ionizer surface as $F = \beta V$. The simulation was performed with different tip radii, r, and at different values of d, as shown in Fig. 3 (a) and Fig. 3 (b), respectively. From the model, we confirmed that β is inversely proportional to r^n and from the best-fit line, we obtained (1):

$$\beta(r) = \frac{252}{r^{0.685}}, \quad d = 50\ \ \mu\text{m} \tag{1}$$

From Fig. 3 (a), we found that $\beta > 0.1$ nm^{-1} are achievable when $r < 7$ nm. β was steady when $d > 50$ μm and a power-law relation was used to fit β with d (2):

$$\beta(d) = 1.22 \times 10^8 + \frac{9.33}{d^{1.25}}, \quad r = 5\ \ \text{nm} \tag{2}$$

Similar trends were observed for different r, but were not shown here for clarity. In our experiments, d was in the mm range due to the low precision in the positioning of the anode. While d would have minimal impact on the ionization voltage, it could influence the ion acceleration towards the anode. In practice, F might not be uniform throughout the tunneling barrier when $r < 10$ nm and β would rise at a smaller rate.

B. Field Emission

In FE mode, I-V characteristics of the fabricated Si FIAs devices were measured to fit the experimental data with the Murphy-Good (MG) equation [26], which corrected a significant error in the original Fowler-Nordheim (FN) equation [27]. The anode current, $I_{\rm A}$, in FE mode is given by (3):

$$I_{\rm A} = a_{\rm FN} V_{\rm GE}^2 \exp\left(-\frac{b_{\rm FN}}{V_{\rm GE}}\right) \tag{3}$$

where $\ln(a_{\rm FN})$ is the intercept and $b_{\rm FN}$ is the absolute value of the slope of the FN plot ($\ln(I/V^2)$ against $1/V$). The relation between $b_{\rm FN}$ and β is given by (4):

$$b_{\rm FN} = \frac{s_{\rm SN} \cdot B \cdot \phi^{\frac{3}{2}}}{\beta} \tag{4}$$

where ϕ is the work function, which can be approximated to the electron affinity, $\chi_{\rm Si}$, of *n*-type Si (4.05 eV), which also leads to the slope correction factor, $s_{\rm SN}$, of about 0.95, and B is a constant in the FN formulation with a value of 6.83 eV$^{-3/2}$·V·nm^{-1} [27]. FE measurements from a typical 1000×1000 array (Fig. 4) demonstrated $I_{\rm A} > 3$ mA at $V_{\rm GE}$ of 60 V, with a turn-on voltage of ∼21 V and anode $b_{\rm FN}$ values of ∼490 V. From (1) and (4), this $b_{\rm FN}$ corresponded to $\beta \approx 0.11$ nm^{-1} and $r \approx 6$ nm. Furthermore, the devices had very low gate leakage with ∼98% transmission to the anode. The gate current, $I_{\rm G}$, also had FN behavior (the inset of Fig. 4), due to the interception of electrons emitted at a wider angle.

C. Field Ionization

Depending on F, the ion current, $I_{\rm Ion}$, consists of two distinct regimes: the *supply limited regime* where all molecules close to the tip are ionized with, $I_{\rm Ion}$ being dependent on the rate of arrival of molecules; and a *field-limited regime* where F is relatively low, with the rate of ionization being smaller than the rate of arrival. At low $V_{\rm EG}$, we are operating in the latter case, and using Wentzel-Kramer-Brillouin (WKB) approximation, the tunneling probability, D, is given by (5) [28]:

$$D \cong \exp\left[-\frac{B(\nu_{\rm FI} E_{\rm I}^{\frac{3}{2}} - \phi^{\frac{3}{2}})}{\beta V_{\rm EG}}\right] \tag{5}$$

where $E_{\rm I}$ is the first ionization energy of the gas, and $\nu_{\rm FI}$ is the value of the special elliptic function, $v(x)$, for $x = f'$. $\nu_{\rm FI}$ and f' are given by (6) and (7), respectively [27]:

$$\nu_{\rm FI} \approx 1 - f' + (1/6) f' \ln f' \tag{6}$$

$$f' = (q^3/\pi\epsilon_0) E_{\rm I}^{-2} \beta V_{\rm EG} \tag{7}$$

where q is the elementary charge, and ϵ_0 is the free-space permittivity. The local ionization density $\mathrm{d}J/\mathrm{d}\Omega$ with position, R, from the center of the gas atom is given by $qC(R)P_e(R)$ where $C(R)$ is the local number density of gas molecules, and $P_e(R) \approx \nu_e D$ is the tunneling rate constant, with ν_e being the tunneling attempt frequency. $I_{\rm Ion}$ is determined by integrating the volume element, $\mathrm{d}\Omega = 2\pi r^2 \mathrm{d}r$, over a hemisphere (8):

$$I_{\rm Ion} = 2\pi \int_{r_c}^{\infty} \frac{\mathrm{d}J}{\mathrm{d}\Omega} \cdot r^2 \mathrm{d}r \approx 2\pi r_c^2 \delta q \nu_e C_{\rm crit} D \tag{8}$$

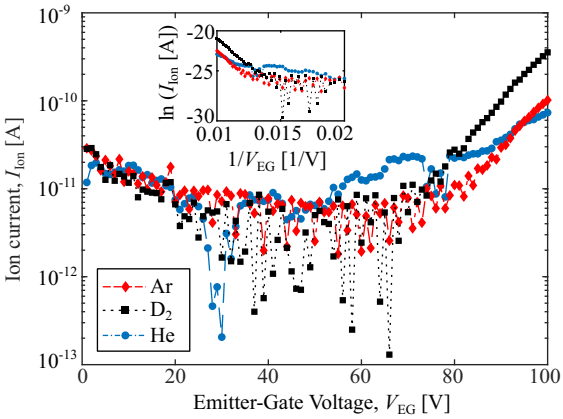

Fig. 5. Field ionization I-V characteristics at around 1 mTorr pressure with Ar, D_2 and He using a 1000×1000 array displaying $I_{\rm Ion}$ at different $V_{\rm EG}$ bias and $V_{\rm A}$ of −200 V. Inset shows the Millikan-Lauritsen (ML) plot demonstrating similar slopes for D_2 and Ar, and smaller slope for He.

where r_c is the radius of the critical surface, and δ is the effective zone width, estimated by $\Delta E/qF$, where ΔE is half-width of the measured total FI energy distribution [29]. For gases with high $E_{\rm I}$, δ is a few tens of pm, hence the atom needs to be in proximity to the ionizer. $C_{\rm crit}$ is the gas concentration in the critical ionization zone and is related to gas concentration in the field-free region, $C_{\rm g}$, by $C_{\rm g}\exp(\alpha_{\rm g}F^2/2kT)$, where $\alpha_{\rm g}$ is the polarizability of the gas, k is the Boltzmann's constant and T is the temperature [29]. The $\alpha_{\rm g}$ for gases used in this work are small [30], hence for $F < 15$ V·nm^{-1}, the dependence of $C_{\rm crit}$ on $V_{\rm EG}$ will be ignored for simplicity.

At around 1 mTorr, we measured the $I_{\rm Ion}$ from the Si FIAs for $V_{\rm EG} < 100$ V as shown in Fig. 5. With all three gases investigated, we obtained threshold voltages, $V_{\rm ON}$, for ionization between 70 V and 85 V. The dependence of $I_{\rm Ion}$ on $V_{\rm EG}$, from (8) can be re-arranged to a Millikan-Lauritsen (ML) [31] plot given by (9):

$$I_{\rm A} = a_{\rm ML}\exp\left(-\frac{b_{\rm ML}}{V_{\rm EG}}\right) \tag{9}$$

where $\ln(a_{\rm ML})$ is the intercept and $b_{\rm ML}$ is the magnitude of the slope of a ML plot ($\ln(I)$ against $1/V$). From (8), if we assume $C_{\rm crit}$ and δ to be constants, $b_{\rm ML}$ is given by (13):

$$b_{\rm ML} = -\frac{{\rm d}\ln I}{{\rm d}V^{-1}} \approx \frac{B}{\beta}\left[\left({\rm v_{FI}} - V\frac{{\rm dv_{FI}}}{{\rm d}V}\right)E_{\rm I}^{\frac{3}{2}} - \phi^{\frac{3}{2}}\right] \tag{10}$$

Using the special mathematical function $s(x)$ given by (11) and the approximation for $s(x)$ given by (12) from [27]:

$$s(x) = v(x) - x{\rm d}v/{\rm d}x \tag{11}$$

$$s(x) \approx 1 - x/6. \tag{12}$$

and assuming ${\rm s_{FI}} = s(f')$, $b_{\rm ML}$, at low F, becomes (13):

$$b_{\rm ML} \approx \frac{B({\rm s_{FI}}E_{\rm I}^{\frac{3}{2}} - \phi^{\frac{3}{2}})}{\beta} \tag{13}$$

The slope correction factor, ${\rm s_{FI}}$, is approximately 0.95 for F between 10 V·nm^{-1} and 15 V·nm^{-1}, considering that $E_{\rm I}$ for Ar, He, and D_2 are 15.8 eV, 24.6 eV, and 14.9 eV, respectively. Since β is same for both FE and FI, we calculated the approximate $b_{\rm ML}$, in Table I using (13). A substantial discrepancy between the calculated and the experimental $b_{\rm ML}$ values (inset of Fig. 5) was found in both possible cases considered: electrons from the atom tunnel in the Si conduction band, $E_{\rm C}$, with $\phi \approx \chi$, and electrons tunnel into the Si valence band, $E_{\rm V}$, with $\phi \approx \chi + E_{\rm G}$ where $E_{\rm G}$ is the Si band-gap of 1.12 eV. The latter situation is shown in Fig. 6 where the field penetration in the Si causes an upward band-bending, $\phi_{\rm S} = qF\lambda/\epsilon_{\rm r}$, where $\epsilon_{\rm r}$ and λ are the relative permittivity of the Si and the penetration depth, respectively [11], [32]. At high F, $\phi_{\rm S}$ could be larger than $E_{\rm G}$, hence unfilled states exist below $E_{\rm V}$ (Fig. 6 (a)). Although $\phi_{\rm S}$ increases the local ϕ and hence D, it does not compensate for the large difference in the $b_{\rm ML}$ from (13) at low $V_{\rm EG}$. If the voltage dependence of $C_{\rm crit}$ from (8) is accounted for in (10), the values of $b_{\rm ML}$ become even larger. Alternative mechanisms such as unfilled local surface states near the Fermi-level (Fig. 6 (b)) could explain the slope difference, as there would be more tunneling sites for FI, even at lower F [11]. The surface charge density, $\sigma_{\rm S}$, also causes shielding and reduces the $\phi_{\rm S}$ by $(\sigma_{\rm S}/(\epsilon_0\epsilon_{\rm r}))$.

TABLE I
COMPARISON OF FI PARAMETERS AT APPROXIMATELY 1 MTORR

Gas	$I_{\rm Ion}$ [nA] @ 100 V	$V_{\rm ON}$ [V]	Measured $b_{\rm ML}$ [V]	Calculated $b_{\rm ML}$ [V]	
				χ	$\chi + E_{\rm G}$
D_2	0.36	72	917	2890	2670
Ar	0.10	75	990	3200	2980
He	0.07	82	631	6690	6470

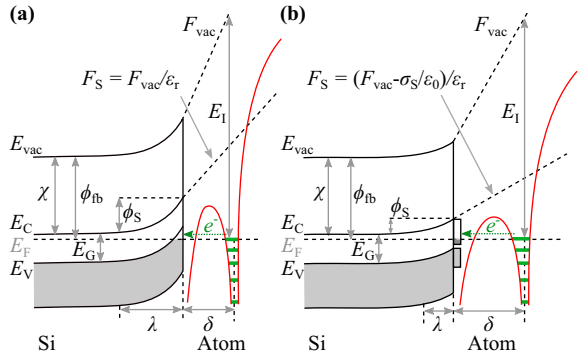

Fig. 6. (a) Energy band diagram in FI mode for *n*-type Si with band bending due to the applied field, $F_{\rm vac}$, in the absence of surface states. (b) Effect of unfilled surface states near the conduction band, with reduced band bending due to surface state shielding allowing FI at lower fields. Not to scale.

The dependence of $I_{\rm Ion}$ on p (1.6 mTorr, 8 mTorr and 16 mTorr), is shown in Fig. 7 (a). The measured $I_{\rm Ion}$ at $V_{\rm EG} =$ 100 V increased linearly with p: from 0.11 nA at $p = 1.6$ mTorr to 0.21 nA at $p = 8.0$ mTorr and to 0.46 nA at $p =$ 16 mTorr. The intercept, $\ln(a_{\rm ML})$, also increased as p rose from 1.6 mTorr to 16 mTorr, while the slopes $b_{\rm ML}$ (∼900) were similar (inset of Fig. 7 (a)). This was expected, as at higher pressure, $C_{\rm g}$ increases and more neutrals reach the tip, hence the local ionization density rises. We achieved higher $I_{\rm Ion}$ by sweeping $V_{\rm EG}$ up to 150 V, increasing $V_{\rm A}$ to −1100 V,

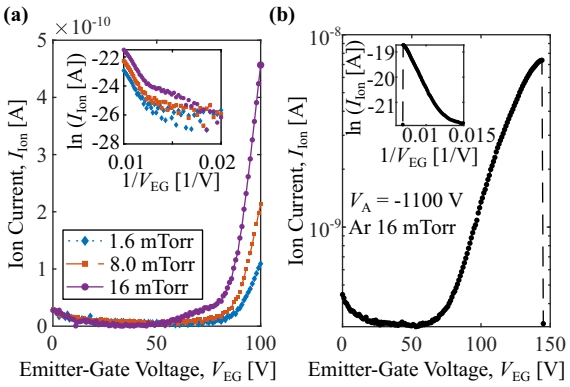

Fig. 7. (a) Effect of Ar pressure on ion current measured by sweeping the emitter-gate voltage from 0 V to 100 V, demonstrating an increase in the ionization current with higher pressure. Inset shows the ML plots of the ion current at different pressures, having similar slopes but different intercepts. (b) High ion current of ∼7 nA observed with Ar at 16 mTorr and high anode voltage of −1100 V. Inset shows the ML plot for the ion current, with slope magnitude, b_{ML}, of 785 V and intercept, $\ln(a_{\mathrm{ML}})$, of −14.4.

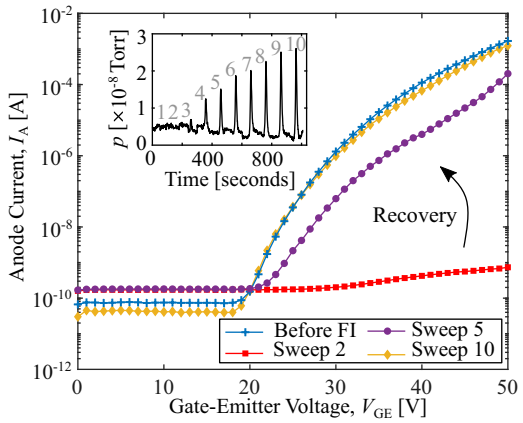

Fig. 8. I-V sweep evolution with V_{GE} from 0 to 50 V showing recovery in performance similar to that before FI after four sweeps in the FE mode. Inset shows evolution of pressure with each sweep with a sudden increase during the 3rd sweep, coinciding with FE recovery.

and using 16 mTorr Ar pressure. This is shown in Fig. 7 (b) where I_{Ion} as high as 7 nA were observed at $V_{\mathrm{EG}} = 147$ V. However, the intense F between the tip and the gate likely caused a stronger acceleration of the ions towards the gate. The impact of the ions on the gate damaged the apertures and consequently, a sudden device failure was observed when $V_{\mathrm{EG}} > 147$ V as shown in Fig. 7 (b).

D. Field Emission Recovery

After FI experiments, the Si FIAs did not immediately recover the FE performance measured at the outset. Instead, multiple V_{GE} sweeps were needed to obtain the original I_{A} as shown in Fig. 8. A key observation was the change in pressure during the sweeps (inset of Fig. 8), where a sudden pressure rise was recorded on the third sweep, after which the FE performance was gradually re-established. Further spikes in the pressure plot (inset of Fig. 8), after the third sweep are due to the increase in the anode current and the high voltage (+1100 V) leading to Joule heating of the anode, and hence, out-gassing in the measurement chamber. The slow FE recovery after FI experiments could be ascribed to either surface adsorption of gas molecules during FI, which prevented electron emission in the initial sweeps in FE mode, or unfilled surface states between the valence and conduction bands, which are depleted during FI [33]. A possible solution was investigated by using of a thin coating of Pt. This layer would serve two purposes: first to improve the gate and tip robustness and secondly, to minimize surface states and surface adsorption of molecules that delay FE recovery.

E. Pt-Coated Ionizers

To compare the FI performance in Ar with coated ionizers, we deposited 5 nm of Pt on the device area using electron beam evaporation. The line-of-sight deposition of Pt enables the ionizers and the gate to be coated without causing an electrical short. The Pt was not sintered due to the possibility

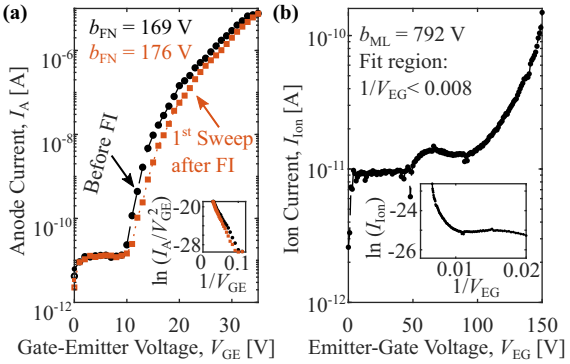

Fig. 9. (a) I-V sweep for Pt coated ionizers in FE mode before and after field ionization with V_{GE} from 0 to 35 V showing performance recovery in the first sweep after FI. Inset shows the FN plots with similar slopes of about −170 V. (b) FI performance in Ar at 16 mTorr and −1100 V anode demonstrating significantly lower current and ML slope of approximately −792 V.

modifying the tip by the movement of Pt and Si atoms. The performance is measured both in FE and FI modes (Fig. 9).

Higher I_{A} in FE measurement (Fig. 9 (a)) of the Pt coated devices were measured compared to uncoated Si tips and therefore, the sweep was performed with V_{GE} of up to 35 V only, to prevent damage at higher voltages caused by anode out-gassing. The considerably lower b_{FN} values of ∼170 V extracted from FN plots (inset of Fig. 9 (a)), and high β of 0.44 nm^{-1} ($\phi = 5.1$ eV) caused a lower turn-on voltage of ∼10 V. This could be due to the formation of sharper tips as Pt might agglomerate into nanoparticles on the tips. As shown in Fig. 9 (a), FE was recovered immediately (1st sweep) after FI when using Pt coated tips compared to pristine Si tips.

In FI measurement with Ar at 16 mTorr illustrated in Fig. 9 (b), we measured I_{Ion} of up to 0.1 nA only, at $V_{\mathrm{EG}} = 150$ V. Although a larger I_{Ion} was expected due to the high β, this was not the case. This could be because of the poor adsorption properties of Pt. At lower fields, molecular adsorption on the shank of the ionizer and their migration towards the ionizer apex are crucial for FI action [11]. By contrast, at higher V_{EG}, the ionization probability of molecules randomly moving in the vicinity of the ionizer becomes significant. Hence, with

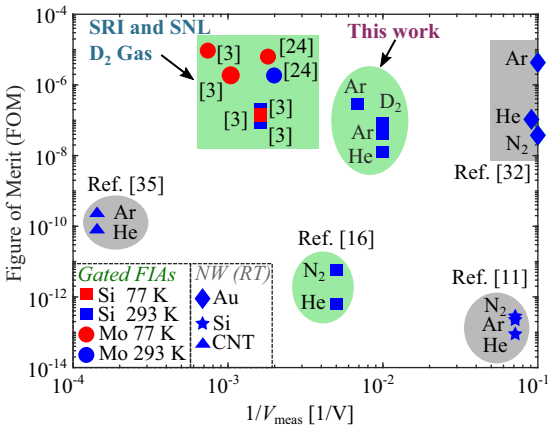

Fig. 10. Performance comparison of previous works on gated (green shade) devices for both Mo (circles) and Si (squares), un-gated (grey shade) Au NW (diamonds), Si nanowhiskers (stars) and CNTs (triangles) measured with high ionization energy gases and at two different temperatures (77 K (red) and room temperature (RT), 293 K (blue)).

a Pt layer, which could also fill the surface states both in FE and FI modes, the surface adsorption mechanism would be ineffective. This was shown by comparing the measured and calculated b_{ML} values. From (13), the calculated b_{ML} was 782 V for Pt coated ionizers, based on the measured β in FE and, using the value of 5.1 eV for ϕ. The corresponding b_{ML} extracted experimentally was 792 V from Fig. 9 (b).

F. Performance Comparison

To compare FIAs from different reports, independent of p, T, molecular mass, m, and device area, A, we calculate the ratio of the flux density of ions, $\mathrm{F_{Ion}}$, produced to the flux density of atoms in field-free space away from the ionizer, $\mathrm{F_{Atom}}$. Assuming each ion at the anode receives an electron, $\mathrm{F_{Ion}}$ is given by (14):

$$\mathrm{F_{Ion}} = \frac{I_{\mathrm{Ion}}}{qA} = \frac{J_{\mathrm{Ion}}}{q} \tag{14}$$

where J_{Ion} is the ion current density at the measured voltage, V_{meas}. From the kinetic theory of gases, $\mathrm{F_{Atom}}$ is given by (15) [34]:

$$\mathrm{F_{Atom}} = \frac{p}{\sqrt{2\pi mkT}} \tag{15}$$

The figure-of-merit (FOM), which is essentially the global ionization efficiency of the array, but not accounting for the molecule polarizability, is given by (16):

$$\mathrm{FOM} = \frac{\mathrm{F_{Ion}}}{\mathrm{F_{Atom}}} = \frac{\sqrt{2\pi k}}{q}\frac{J_{\mathrm{Ion}}\sqrt{mT}}{p} \tag{16}$$

Data collected from previous works on gated FIAs [3], [16], [24], un-gated CNT forests [35], dense Au NW [32], and undoped-Si nanowhiskers [11] have been used to calculate FOM values at V_{meas} as illustrated in Fig. 10.

While un-gated NW and nanowhiskers in [11], [32] demonstrated ultra-low ionization voltages, gated FIAs have the advantage of using different voltages for ionization and acceleration. Gated FIAs based on W-coated Si tips from Sandia National Laboratories (SNL) and Mo Spindt cathodes from SRI International demonstrated improved FI at lower temperatures of 77 K [3], [24]. The bias needed to achieve similar FOM values in this work, were significantly smaller (<200 V) as illustrated in Fig. 10. A lower T could also enhance adsorption of molecules on the surface of our Si FIAs and increase I_{Ion} compared to measurements at 293 K. Material adsorption properties are also not quantified in (16); further analysis may be needed to compare different tip material [29]. Nonetheless, FIAs fabricated in this work with higher tip density (10^8 cm^{-2}) and narrower aperture diameter (∼350 nm), demonstrated higher FOM, compared to Fomani *et al.* [16], with gated, Pt-coated Si FIAs with smaller tip densities (10^6 cm^{-2}) and, wider aperture diameter (1 µm). Consistent and high I_{Ion} at low V_{EG}, would require a coating with higher adsorption efficiency such as Ti, and a rougher ionizer for a larger surface area. Additionally, a low-duty voltage pulsing mechanism could allow a settling time for surface adsorption of molecules. In uncoated Si tips, pulsing V_{EG} could likewise speed up FE recovery, with ionization in the reverse bias and desorption of molecules from the tip in the forward bias.

IV. Conclusion

Dense gated Si nano-tip arrays (10^8 cm^{-2}) with integrated NW current-limiters and self-aligned apertures were fabricated and characterized in both FE and FI modes. We demonstrated high β at the tip exceeding 0.1 nm^{-1} in FE mode. These high β considerably reduce the bias necessary to ionize gases (Ar, D_2 and He), with high first ionization energy. We achieved I_{Ion} of ∼0.4 nA at a moderate bias of 100 V and demonstrated linearity with pressure in the range studied. Initial FE performance was recovered after multiple V_{GE} sweeps. We measured higher I_{Ion} of 7 nA at ∼147 V, but to the detriment of the gate integrity. With a thin Pt layer, we obtained higher β, yet lower I_{Ion}, hinting at the effects of surface states or molecular adsorption and their migration being dominant at lower fields in pristine Si tips. We envision that these low-voltage Si FIAs can find multitude of applications including mass spectrometry, ion mobility spectrometry, neutron generators and sensors.

Acknowledgement

This work was carried out in part through the use of MIT's Microsystems Technology Laboratories (MTL) and MIT.nano. Funding from the Defense Advanced Research Projects Agency (DARPA) under the cooperative agreement number: HR0011-15-20012 is duly acknowledged.

References

[1] E. W. Müller, "Study of atomic structure of metal surfaces in the field ion microscope," *Journal of Applied Physics*, vol. 28, no. 1, pp. 1–6, Jan. 1957. [Online]. Available: https://dx.doi.org/10.1063/1.1722557

[2] H.-D. Beckey, *Principles of Field Ionization and Field Desorption Mass Spectrometry*. Oxford: Pergamon, 1977.

[3] B. B. Johnson, P. R. Schwoebel, P. J. Resnick, C. E. Holland, K. L. Hertz, and D. L. Chichester, "Field ionization characteristics of an ion source array for neutron generators," *Journal of Applied Physics*, vol. 114, no. 17, p. 174906, Nov. 2013. [Online]. Available: https://dx.doi.org/10.1063/1.4826111

[4] P. A. Sohi and M. Kahrizi, "Low-voltage gas field ionization tunneling sensor using silicon nanostructures," *IEEE Sensors Journal*, vol. 18, no. 15, pp. 6092–6096, Aug. 2018. [Online]. Available: https://dx.doi.org/10.1109/jsen.2018.2846254

[5] E. W. Müller and T. T. Tsong, *Field ion microscopy: Principles and applications*. American Elsevier Publishing Company, 1969.

[6] M. Barr, A. Fahy, J. Martens, A. P. Jardine, D. J. Ward, J. Ellis, W. Allison, and P. C. Dastoor, "Unlocking new contrast in a scanning helium microscope," *Nature Communications*, vol. 7, no. 1, Jan. 2016. [Online]. Available: https://dx.doi.org/10.1038/ncomms10189

[7] R. Gomer, *Field emission and field ionization*, ser. Harvard monographs in applied science. Harvard University Press, 1961.

[8] K. H. Becker and V. Tarnovsky, "Electron-impact ionization of atoms, molecules, ions and transient species," *Plasma Sources Science and Technology*, vol. 4, no. 2, pp. 307–315, May 1995. [Online]. Available: https://dx.doi.org/10.1088/0963-0252/4/2/015

[9] F. H. Field, "Chemical ionization mass spectrometry," *Accounts of Chemical Research*, vol. 1, no. 2, pp. 42–49, Feb. 1968. [Online]. Available: https://dx.doi.org/10.1021/ar50002a002

[10] D. M. Hindenlang and R. D. Sedgwick, "Mass spectrometry," in *Comprehensive Polymer Science and Supplements*. Elsevier, 1989, pp. 573–588. [Online]. Available: https://dx.doi.org/10.1016/b978-0-08-096701-1.00026-4

[11] R. B. Sadeghian and M. S. Islam, "Ultralow-voltage field-ionization discharge on whiskered silicon nanowires for gas-sensing applications," *Nature Materials*, vol. 10, no. 2, pp. 135–140, Jan. 2011. [Online]. Available: https://dx.doi.org/10.1038/nmat2944

[12] M. K. Miller, A. Cerezo, M. G. Hetherington, and G. D. W. Smith, *Atom probe field ion microscopy*. Oxford University Press, 1996.

[13] C. M. Lyneis, "Performance of present high charge state ECR ion sources and challenges for next generation sources," in *2012 Abstracts IEEE International Conference on Plasma Science*. IEEE, Jul. 2012. [Online]. Available: https://dx.doi.org/10.1109/plasma.2012.6383981

[14] C. A. Spindt, "A thin-film field-emission cathode," *Journal of Applied Physics*, vol. 39, no. 7, pp. 3504–3505, Jun. 1968. [Online]. Available: https://dx.doi.org/10.1063/1.1656810

[15] A. Persaud, I. Allen, M. R. Dickinson, T. Schenkel, R. Kapadia, K. Takei, and A. Javey, "Development of a compact neutron source based on field ionization processes," *Journal of Vacuum Science & Technology B, Nanotechnology and Microelectronics: Materials, Processing, Measurement, and Phenomena*, vol. 29, no. 2, p. 02B107, Mar. 2011. [Online]. Available: https://dx.doi.org/10.1116/1.3531929

[16] A. A. Fomani, L. F. Velasquez-Garcia, and A. I. Akinwande, "Low-voltage field ionization of gases up to Torr-level pressures using massive arrays of self-aligned gated nanoscale tips," *IEEE Transactions on Electron Devices*, vol. 61, no. 5, pp. 1520–1528, May 2014. [Online]. Available: https://dx.doi.org/10.1109/ted.2014.2310637

[17] K. L. Jensen, E. G. Zaidman, M. A. Kodis, B. Goplen, and D. N. Smithe, "Analytical and seminumerical models for gated field emitter arrays. I. Theory," *Journal of Vacuum Science & Technology B: Microelectronics and Nanometer Structures*, vol. 14, no. 3, p. 1942, May 1996. [Online]. Available: https://dx.doi.org/10.1116/1.588960

[18] K. G. Polat, C. Zhou, A. Umar, and M. S. Islam, "Optimized ultrasharp silicon nanowire geometries for enhanced field ionization properties," *MRS Proceedings*, vol. 1785, pp. 7–11, 2015. [Online]. Available: https://dx.doi.org/10.1557/opl.2015.514

[19] S. A. Guerrera, L. F. Velasquez-Garcia, and A. I. Akinwande, "Scaling of high-aspect-ratio current limiters for the individual ballasting of large arrays of field emitters," *IEEE Transactions on Electron Devices*, vol. 59, no. 9, pp. 2524–2530, Sep. 2012. [Online]. Available: https://dx.doi.org/10.1109/ted.2012.2204262

[20] N. Karaulac, G. Rughoobur, and A. I. Akinwande, "Highly uniform silicon field emitter arrays fabricated using a trilevel resist process," *Journal of Vacuum Science & Technology B*, vol. 38, no. 2, p. 023201, Mar. 2020. [Online]. Available: https://dx.doi.org/10.1116/1.5131656

[21] G. Rughoobur and A. I. Akinwande, "Arrays of Si field emitter individually regulated by Si nanowires - High breakdown voltages and enhanced performance," in *2018 31st International Vacuum Nanoelectronics Conference (IVNC)*. IEEE, Jul. 2018. [Online]. Available: https://dx.doi.org/10.1109/ivnc.2018.8520086

[22] S. A. Guerrera and A. I. Akinwande, "Nanofabrication of arrays of silicon field emitters with vertical silicon nanowire current limiters and self-aligned gates," *Nanotechnology*, vol. 27, no. 29, p. 295302, Jun. 2016. [Online]. Available: https://dx.doi.org/10.1088/0957-4484/27/29/295302

[23] M. Ding, G. Sha, and A. I. Akinwande, "Silicon field emission arrays with atomically sharp tips: turn-on voltage and the effect of tip radius distribution," *IEEE Transactions on Electron Devices*, vol. 49, no. 12, pp. 2333–2342, Dec. 2002. [Online]. Available: https://dx.doi.org/10.1109/ted.2002.805230

[24] B. B. Johnson, P. R. Schwoebel, C. E. Holland, P. J. Resnick, K. L. Hertz, and D. L. Chichester, "Field ion source development for neutron generators," *Nuclear Instruments and Methods in Physics Research Section A: Accelerators, Spectrometers, Detectors and Associated Equipment*, vol. 663, no. 1, pp. 64–74, Jan. 2012. [Online]. Available: https://dx.doi.org/10.1016/j.nima.2011.09.034

[25] F. Paschen, "Ueber die zum funkenübergang in luft, wasserstoff und kohlensäure bei verschiedenen drucken erforderliche potentialdifferenz," *Annalen der Physik*, vol. 273, no. 5, pp. 69–96, 1889. [Online]. Available: https://dx.doi.org/10.1002/andp.18892730505

[26] E. L. Murphy and R. H. Good, "Thermionic Emission, Field Emission, and the Transition Region," *Physical Review*, vol. 102, no. 6, pp. 1464–1473, Jun. 1956. [Online]. Available: https://dx.doi.org/10.1103/physrev.102.1464

[27] R. G. Forbes and J. H. B. Deane, "Reformulation of the standard theory of Fowler–Nordheim tunnelling and cold field electron emission," *Proceedings of the Royal Society A: Mathematical, Physical and Engineering Sciences*, vol. 463, no. 2087, pp. 2907–2927, Aug. 2007. [Online]. Available: https://dx.doi.org/10.1098/rspa.2007.0030

[28] B. Halpern and R. Gomer, "Field ionization in liquids," *The Journal of Chemical Physics*, vol. 51, no. 3, pp. 1048–1056, Aug. 1969. [Online]. Available: https://dx.doi.org/10.1063/1.1672103

[29] R. G. Forbes, "Gas field ionization sources," in *Handbook of Charged Particle Optics*. CRC Press, Dec. 2017, pp. 87–128. [Online]. Available: https://dx.doi.org/10.1201/9781420045550-3

[30] ——, "Atomic polarisability values in the SI system," *Surface Science*, vol. 64, no. 1, pp. 367–371, apr 1977. [Online]. Available: https://dx.doi.org/10.1016/0039-6028(77)90283-7

[31] R. A. Millikan and C. C. Lauritsen, "Relations of field-currents to thermionic-currents," *Proceedings of the National Academy of Sciences*, vol. 14, no. 1, pp. 45–49, Jan. 1928. [Online]. Available: https://dx.doi.org/10.1073/pnas.14.1.45

[32] R. B. Sadeghian and M. Kahrizi, "A novel gas sensor based on tunneling-field-ionization on whisker-covered gold nanowires," *IEEE Sensors Journal*, vol. 8, no. 2, pp. 161–169, Feb. 2008. [Online]. Available: https://dx.doi.org/10.1109/jsen.2007.912788

[33] H. Karaagac and M. S. Islam, "Enhanced field ionization enabled by metal induced surface states on semiconductor nanotips," *Advanced Functional Materials*, vol. 24, no. 15, pp. 2224–2232, Dec. 2013. [Online]. Available: https://dx.doi.org/10.1002/adfm.201303308

[34] R. Fowler and E. A. Guggenheim, *Statistical thermodynamics*. Cambridge University Press, 1952.

[35] J. Luo, L. P. Mark, A. E. Giannakopulos, A. W. Colburn, J. V. Macpherson, T. Drewello, P. J. Derrick, A. S. Teh, K. B. K. Teo, and W. I. Milne, "Field ionization using densely spaced arrays of nickel-tipped carbon nanotubes," *Chemical Physics Letters*, vol. 505, no. 4-6, pp. 126–129, Mar. 2011. [Online]. Available: https://dx.doi.org/10.1016/j.cplett.2011.02.028